High Resolution Nonoscillatory Central Difference Schemes for the 2D Euler Equations via Artificial Compression

K.-A. Lie[1] and S. Noelle[2]

[1] SINTEF Applied Mathematics, P.0. Box 124 Blindern, N–0314 Oslo, Norway
[2] Institut für Geometrie und Praktische Mathematik, RWTH Aachen, D-52056 Aachen, Germany

Abstract. We suggest to augment second-order, nonoscillatory, central difference schemes with Harten's artificial compression method (ACM) to sharpen the resolution of linear fields. ACM employs a partial characteristic decomposition to single out the linear fields, for which a steeper reconstruction is applied. The remarkable power of this technique is demonstrated for three test problems for the Euler equations from gas dynamics, and its dangers are pointed out.

1 Introduction

High-resolution methods for conservation laws can roughly be divided into two classes; upwind and central difference methods. By far the most popular are the upwind methods, which are based upon an idea dating back to Godunov. The common feature of this class is the use of Riemann solvers and incorporation of characteristic information. The upwind methods therefore give very sharp resolution of discontinuities, but are quite complicated and require extensive knowledge of the system to be solved.

Recently, central methods, which go back to the famous Lax–Friedrichs scheme [1], have experienced a widespread revival, inspired by the work of Nessyahu and Tadmor [2]. These schemes apply no characteristic information or Riemann solvers and therefore yield especially compact and simple computer code. However, the schemes have a tendency of smearing linear discontinuities more than the upwind schemes. To amend this problem, Nessyahu and Tadmor [2] suggested two methods to improve their one-dimensional scheme: Apply Harten's ACM [3] to the reconstruction of the linear fields only, or alternatively, apply a corrector step to all components of the conservative variables.

Here we study the two-dimensional extension of the Nessyahu–Tadmor scheme [4,5] as modified in [6], which we augment by the ACM method to improve resolution of linear fields. We thereby adopt one of the successful ideas from the upwind methods and deviate from a basic principle of the central difference schemes since the ACM is based upon a partial characteristic decomposition.

The Nessyahu–Tadmor scheme is based upon evolution of cell averages over a staggered grid, thereby avoiding Riemann problems. Let $x_j = j\Delta x$ and $y_k = k\Delta y$. The grid consists of the original cells $C_{jk} = [x_{j-1/2}, x_{j+1/2}] \times [y_{k-1/2}, y_{k+1/2}]$ at even time steps and the staggered cells $[x_j, x_{j+1}] \times [y_k, y_{k+1}]$ at odd time steps. Assume the following piecewise linear reconstruction at time t_n, n even, over the *original* grid,

$$\overline{w}(x,y,t_n) = \overline{w}_{jk}^{\,n} + \frac{x-x_j}{\Delta x} w'^{x}_{jk} + \frac{y-y_k}{\Delta y} w'^{y}_{jk}, \quad \text{for } (x,y) \in C_{jk},$$

where $\overline{w}_{jk}^{\,n}$ are the cell-averages and the finite difference operators $'^{x} \approx \Delta x \frac{\partial}{\partial_x}$ and $'^{y} \approx \Delta y \frac{\partial}{\partial_y}$ are realised with standard limiter functions. Here we use the WENO limiter

$$\mathrm{WENO}(a,b) = \big(w(a)\cdot a + w(b)\cdot b\big)/\big(w(a)+w(b)\big),$$

where the weights are given by $w(a) = \big(10^{-6} + a^2\big)^{-2}$.

The NT2d scheme computes the update $\overline{w}_{j+1/2,k+1/2}^{\,n+1}$ at time t_{n+1} over the *staggered* cells as

$$\begin{aligned}
\overline{w}_{j+1/2,k+1/2}^{\,n+1} =& \frac{1}{4}\big(\overline{w}_{jk}^{\,n} + \overline{w}_{j+1,k}^{\,n} + \overline{w}_{j+1,k+1}^{\,n} + \overline{w}_{j,k+1}^{\,n}\big) \\
&+ \frac{1}{16}\big(w'_{jk} + w'_{j,k+1} - w'_{j+1,k} - w'_{j+1,k+1}\big) \\
&+ \frac{1}{16}\big(w'^{y}_{jk} - w'^{y}_{j,k+1} + w'^{y}_{j+1,k} - w'^{y}_{j+1,k+1}\big) \\
&- \frac{\lambda}{4}\Big[f(w^{n+1}_{j+1,k}) + f^{n,-}_{j+1,k+1/2} + f^{n,+}_{j+1,k+1/2} + f(w^{n+1}_{j+1,k+1})\Big] \\
&+ \frac{\lambda}{4}\Big[f(w^{n+1}_{jk}) + f^{n,-}_{j,k+1/2} + f^{n,+}_{j,k+1/2} + f(w^{n+1}_{j,k+1})\Big] \\
&- \frac{\mu}{4}\Big[g(w^{n+1}_{j,k+1}) + g^{n,-}_{j+1/2,k+1} + g^{n,+}_{j+1/2,k+1} + g(w^{n+1}_{j+1,k+1})\Big] \\
&+ \frac{\mu}{4}\Big[g(w^{n+1}_{jk}) + g^{n,-}_{j+1/2,k} + g^{n,+}_{j+1/2,k} + g(w^{n+1}_{j+1,k})\Big],
\end{aligned}$$

where $\lambda = \Delta t/\Delta x$, $\mu = \Delta t/\Delta y$ and $w^{n+1}_{jk} = \overline{w}_{jk}^{\,n} - \lambda f'_{jk} - \mu g'^{y}_{jk}$, and

$$\begin{aligned}
f^{n,-}_{j,k+1/2} =& f(\overline{w}_{jk}^{\,n} + \frac{1}{2} w'^{y}_{jk}) \approx f(\overline{w}_{jk}^{\,n}) + \frac{1}{2} f'^{y}_{jk}, \\
f^{n,+}_{j,k+1/2} =& f(\overline{w}_{j,k+1}^{\,n} - \frac{1}{2} w'^{y}_{j,k+1}) \approx f(\overline{w}_{j,k+1}^{\,n}) - \frac{1}{2} f'^{y}_{j,k+1},
\end{aligned}$$

and similarly for $g^{n,-}_{j+1/2,k}$ and $g^{n,+}_{j+1/2,k}$.

2 Inclusion of Artificial Compression

The basic idea of the ACM method is to employ a steeper reconstruction of linear fields, see [3,2]. To compute the numerical x-derivatives of the conservative variables, w'^{x}, over cell C_{jk} using ACM we first introduce a Roe matrix

$\hat{A}$ (an averaged Jacobian) satisfying $f(w_{j+1,k}) - f(w_{jk}) = \hat{A}_{jk}(w_{j+1,k} - w_{jk})$. For each $\hat{A}$ we assume a characteristic decomposition

$$\Delta w_{jk} = w_{j+1,k} - w_{jk} = \sum_i \alpha^i_{jk} R^i_{jk},$$

i.e., a projection onto the right eigenvectors R^i_{jk}. To exemplify, we consider the Euler equations of gas dynamics for an ideal, polytropic gas. In two space-dimensions there are two linear fields, corresponding to a contact and a shear wave. We separate the projections onto both fields from the vector of differences, $\Delta\tilde{w}_{jk} = \Delta w_{jk} - \sum_{i=2,3} \alpha^i_{jk} R^i_{jk}$. Based upon this partial characteristic decomposition, the numerical derivative can be written as

$$w'^x_{jk} = L(\Delta\tilde{w}_{j-1,k}, \Delta\tilde{w}_{jk}) + \sum_{i=2,3} L(\alpha^i_{j-1,k}, \alpha^i_{jk}) R^i_{jk}.$$

We are now in a position to apply the ACM reconstruction to each of the linear fields, that is, apply a steeper reconstruction of the form

$$\Big(L(\alpha^i_{j-1,k}, \alpha^i_{jk}) + \theta_{jk} r_{jk}\Big) R^i_{jk}, \qquad \theta^i_{jk} = \frac{|\alpha^i_{jk} - \alpha^i_{j-1,k}|}{|\alpha^i_{jk}| + |\alpha^i_{j-1,k}|}.$$

Similarly as in [3, (5.8b)], we use

$$r^i_{jk} = \sigma L\Big(q(\lambda\hat{u}_{j+1/2,k})\hat{\alpha}^i_{j+1/2,k}, q(\lambda\hat{u}_{j-1/2,k})\hat{\alpha}^i_{j-1/2,k}\Big),$$

where σ is a constant, $\hat{u}$ is the Roe-averaged x-velocity, $q(\nu) = 1 - \nu^2/2$. The function L is an even function of $\hat{u}$, so the same amount of artificial compression is applied to waves travelling to the left and right. Analogous recipes are used to steepen f'^x, w'^y and g'^y. We do not apply the ACM to the x-derivative g'^x, since the Roe-decomposition in x-direction is related to f (and its Jacobian), but not to g, which has a different eigensystem. For the same reason, we leave f'^y untouched.

Next, we demonstrate the improved performance of our augmented scheme on three test cases for the Euler equations with gas constant $\gamma = 1.4$.

Example 1 Our first example is a two-dimensional Riemann problem with four constant states, one in each quadrant, see [7, Configuration B]. The solution consists of a vortex moving clockwise, where four contact discontinuities spiral around the center at the origin. Figure 1 shows the self-similar solution (here: at time $t = 0.5$ on the domain $[-1, 1]^2$) computed by the NT2d scheme with and without artificial compression. As in [7] we used a 400×400 grid. Inclusion of ACM leads to a remarkable improvement in the resolution of the four slip lines.

Example 2 In the second example, the initial data are a circular variant of Sod's shock tube problem with (ρ, p, u, v) equal $(1.0, 1.0, 0, 0)$ inside a circle

Table 1. Grid refinement study of L^1 error in the conserved variables for NT2d (top) and NT2d + ACM (bottom). EOC denotes the average estimated order of convergence for each $N \times N$ grid. The CPU times are in seconds on a 450 MHz Intel Pentium II processor

N	ρ	ρu_r	E	u_r	p	CPU
50	5.136e-02	3.821e-02	9.871e-02	1.129e-01	3.928e-02	1.1
100	2.674e-02	2.063e-02	4.937e-02	5.748e-02	2.002e-02	9.4
200	1.456e-02	1.150e-02	2.563e-02	2.743e-02	1.004e-02	70.9
400	8.154e-03	6.590e-03	1.356e-02	1.344e-02	5.148e-03	549.0
EOC:	0.89	0.85	0.95	1.02	0.98	—
50	4.170e-02	3.243e-02	9.016e-02	1.042e-01	3.624e-02	1.5
100	2.126e-02	1.660e-02	4.525e-02	5.267e-02	1.824e-02	12.7
200	1.073e-02	8.385e-03	2.283e-02	2.559e-02	9.135e-03	111.7
400	5.686e-03	4.629e-03	1.244e-02	1.386e-02	4.932e-03	852.7
EOC:	0.96	0.94	0.95	0.97	0.96	—

of radius 0.4 and equal $(0.0125, 0.1, 0, 0)$ outside. The solution consists of a circular shock wave propagating outwards from the origin, followed by a contact discontinuity, and a rarefaction wave travelling towards the origin.

Figure 2 gives scatter plots for the uncompressed and compressed schemes. In the current setting, a scatter plot for a given physical quantity is a plot of the value in each grid cell versus the distance of the cell center from the origin. In this way we can present the spread in the data, as a solution with perfect radial symmetry would consist of points lying on a single line. Contrary to the uncompressed computation (see top of Figure 2), the constant state in the internal energy between the leading shock and the contact discontinuity is resolved well the compressive scheme. Moreover, the number of grid points on which the wave is spread is (almost) the same for the contact and the shock wave.

Figure 3 shows cross-sections of the density around the contact and the shock for varying degrees of ACM. All computations are on a 201×201 grid with fixed CFL number 0.4. The uncompressed scheme ($\sigma = 0$) has six points in the contact, while the most compressed scheme ($\sigma = 2$) shows a sharp one-point profile. This is very satisfactory, since we are dealing with a moving contact discontinuity. Moreover, ACM hardly effects the solution away from the contact discontinuity.

Table 1 reports a grid refinement study for the NT2d scheme with $\sigma = 0.0$ and $\sigma = 2.0$. The errors were estimated relative to the cell average of a very accurate solution of the reduced one-dimensional, inhomogeneous system. We see that by including artificial compression, the error is decreased in all variables at the expense of a 50–70% increase in runtime. As expected the convergence is also improved. If we measure accuracy obtained per unit CPU time, the performance is comparable for the two σ-values.

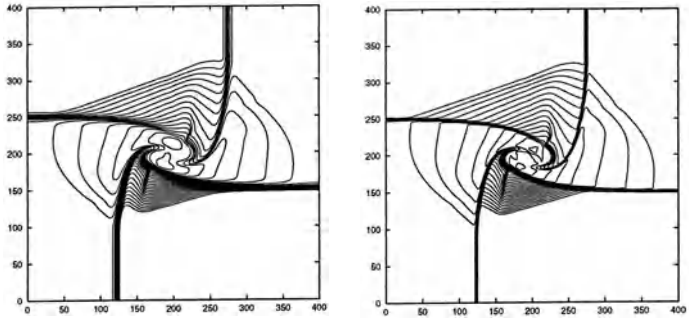

Fig. 1. Density component for solution of two-dimensional Riemann problem; 29 contour lines 0.25 : 0.1 : 3.05. (**a**) uncompressed scheme and (**b**) ACM with $\sigma = 2.0$

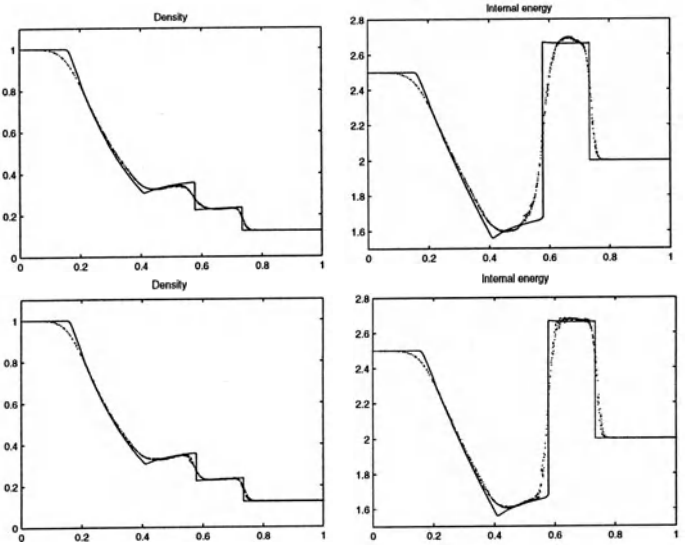

Fig. 2. Scatter plot of the NT2d solution on a 101×101 grid with fixed CFL number 0.475; (top) uncompressed scheme, (bottom) with artificial compression ($\sigma = 2.0$)

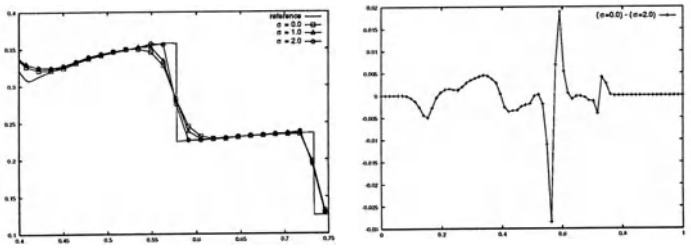

Fig. 3. Density component along the line $x = y$ for $x > 0$. (**a**) Zoom on shock and contact discontinuity. (**b**) Difference in solution computed with uncompressed scheme ($\sigma = 0.0$) and with $\sigma = 2.0$

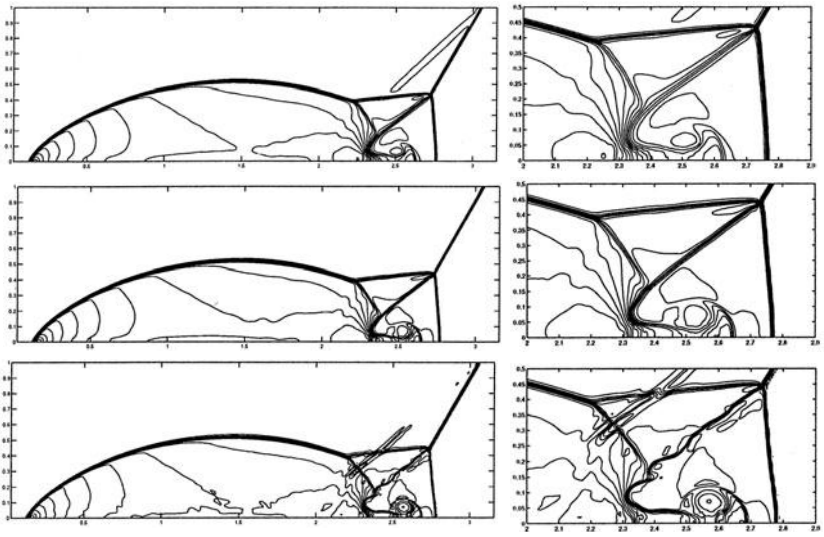

Fig. 4. Double Mach reflection with $\Delta x = 1/200$ for σ equal 0.0, 1.0, and 2.0 from top to bottom

Example 3 Our last example is a classical test problem for gas dynamics, the double Mach reflection problem made popular by Woodward and Colella [8]. Numerical results for the NT2d scheme without artificial compression are reported in [5]. As in [5], we make no effort to optimize the boundary treatment; the same treatment is applied to staggered and non-staggered cells.

Figure 4 shows the density component for simulations with varying degree of artificial compression for $\Delta x = 1/200$ and fixed CFL number 0.475. The artificial compression clearly improves the resolution of the contact wave emanating from the rightmost Mach stem and the jet formed when this wave hits the lower wall. For $\sigma = 2.0$, $\Delta x = 1/200$ we observe how the contact wave becomes unstable and lots of small vortices are created. Although the $\sigma = 2.0$ result strongly resembles highly resolved computations by, e.g., fourth and fifth order WENO schemes, one can question whether the added details are physical or spurious numerical effects.

Concluding Remarks We have demonstrated the power of artificial compression – the ability to sharpen linear waves. This is also the potential danger of the method: it may overcompress smooth linear waves into step-functions and nonlinear rarefaction waves into entropy-violating shocks. In forthcoming work we will present sharp stability estimates and further numerical experiments which will demonstrate these delicate points.

References

1. Lax P. (1954) Weak solutions of nonlinear hyperbolic equations and their numerical computation. Comm. Pure Appl. Math. **7**, 159–193

2. Nessyahu H., Tadmor E. (1990) Non-oscillatory central differencing for hyperbolic conservation laws. J. Comput. Phys. **87**, 408–463
3. Harten A. (1983) High resolution schemes for hyperbolic conservation laws. J. Comp. Phys. **49**, 357–393
4. Arminjon P., Stanescu D., Viallon M.–C. (1995) A two-dimensional finite volume extension of the Lax–Friedrichs and Nessyahu–Tadmor schemes for compressible flows. In: Hafez M., Oshima K. (Eds.) Proc. 6th. Int. Symp. on CFD, Lake Tahoe, Vol. IV, 7–14
5. Jiang G.–S., Tadmor E. (1998) Nonoscillatory central schemes for multidimensional hyperbolic conservation laws. SIAM J. Sci. Comput. **19(6)**, 1892–1917
6. Lie K.–A., Noelle S. (2000) Remarks on high-resolution non-oscillatory central schemes for multi-dimensional systems of conservation laws. Part I: An improved quadrature rule for the flux-computation. Preprint no. 679, Sonderforshugsbereich 256, Rheinische Friedrich–Wilhelms–Unversitat, Bonn, Germany.
7. Schulz–Rinne C. W., Collins J. P., Glaz H. M. (1993) Numerical solution of the Riemann problem for two-dimensional gas dynamics. SIAM J. Sci. Comput. **14(6)**, 1394–1414
8. Woodward P., Colella P. (1984) The numerical simulation of two-dimensional fluid flow with strong shocks. J. Comput. Phys. **54**, 115–173